AIAA JOURNAL
Vol. 34, No. 12, December 1996

Modeling Piezoceramic Actuation of Beams in Torsion

Christopher Park* and Inderjit Chopra†
University of Maryland, College Park, Maryland 20742-3015

A one-dimensional model is developed to predict the coupled extension, bending, and torsion response of a beam subject to piezoceramic strain actuation. The effects of cross-sectional warping are shown to be negligible for thin rectangular isotropic beams. The impact of adhesive shear lag, on the other hand, is measurable, especially in the torsional response. Experimental test results show that the models are accurate up to a 45 deg actuator orientation with respect to the beam axis even though detailed strain data indicate that the local strain state is highly two dimensional.

Nomenclature

A = cross-sectional area
E = Young's modulus, also electric field [V/mil]
G = shear modulus
I = flexural area moment of inertia
J = torsional rigidity constant
L = projected actuator half-length
L_λ = warping parameter
M = bending moment
P = axial force
S = first bending moment of inertia
T = torque
u = axial displacement
v = transverse displacement
w = bending displacement
β = actuator orientation relative to beam axis
Γ = shear lag parameter
γ = shear strain
ε = axial strain
θ = twist rate
κ = bending curvature
Λ = piezoceramic actuation strain
λ = warping function
ν = Poisson's ratio
σ = axial stress
τ = shear stress
ϕ = twist displacement
ψ = stiffness ratio
$\tilde{}$ = actuator axes reference

Superscripts and Subscripts

a = actuator reference
b = beam reference
o = mid-plane reference
s = adhesive substrate reference
κ = bending curvature reference
λ = warping reference
$*$ = effective value

Presented as paper 94-1781 at the AIAA 35th Structures, Structural Dynamics, and Materials Conference and Adaptive Structures Forum, Hilton Head, SC, April 18–21, 1994; received Sept. 21, 1995; revision received June 24, 1996; accepted for publication July 3, 1996; also published in *AIAA Journal on Disc*, Volume 2, Number 1.

*Rotorcraft Fellow; currently Associate Research Engineer, United Technologies Research Centers, East Hartford, CT 06108. Member AIAA.

†Professor of Aerospace Engineering and Director of Center for Rotorcraft Education and Research. Fellow AIAA.

Introduction

HELICOPTERS suffer from excessive vibration, high-fatigue loads, poor handling qualities, and intolerable noise. The objective is to improve the dynamic performance of the helicopter and reduce vibration to an acceptable level. Research on higher harmonic control (HHC)[1,2] and individual blade control (IBC)[3] for helicopter vibration suppression has shown that these concepts can be used to reduce vibration transmitted to the pilot's seat. However, HHC and IBC have high weight penalties and are limited in their application to reduce stresses, improve performance, and reduce noise. It is envisioned that incorporating smart structure technology in rotor blades can give desirable shape-control characteristics to improve the helicopter in all of these areas at a reasonable weight penalty. The need for modeling intelligent structures, in particular beams undergoing combined extension, bending, and torsional deflections due to induced strain actuation, is important in development of smart rotor blades.

Crawley and de Luis[4] presented an analytical uniform strain model of a beam with strain-induced actuation by use of surface-bonded piezoceramics. The model predicted beam extension and bending and included shear lag effects of the adhesive substrate between the piezoceramic and the beam. The dynamic model was experimentally verified for the first two bending modes of a cantilever beam. Crawley and de Luis[5] later presented a uniform strain beam model of both embedded and surface-mounted piezoceramic actuators. They validated the dynamic response at resonance by using aluminum, glass-epoxy, and graphite-epoxy beams. Crawley and Anderson[6] presented a Bernoulli–Euler model and compared it with the previously mentioned uniform strain model, a finite-element model and experiment. All of these models assume a pair of actuators aligned with and symmetrically located with respect to the beam axis. The uniform strain model was quite good except for predicting the response of beams with low-beam-thickness to actuator-thickness ratios. The Bernoulli–Euler model was accurate in predicting both bending and extension responses. Park et al.[7] formulated two additional shear lag models. The first model investigated coupled extension and bending of a rectangular beam with a single piezoceramic bonded to the beam surface and aligned with the beam axis. The second model permitted an arbitrary orientation of the piezoceramic with respect to the beam axis to predict coupled extension, bending, and torsion. Both models utilized a Newtonian shear lag formulation in which the strain was assumed to be constant through the thickness of the actuator and linear through the beam. To maintain a one-dimensional characterization of the problem, the actuator was considered a line element and permitted to induce strain only in its lengthwise axis. Both models were correlated with static deflection data and the bending–extension model was further compared to the Bernoulli–Euler model presented by Crawley and Anderson.[6] The bending–extension model was found to adequately predict the experimental results for various geometric parameters. The coupled extension, bending, and torsion model, however, was capable of capturing only experimental trends, not magnitudes, especially at high actuator orientation angles relative to the beam axis.

Thus, structural modeling of beam extension and bending with embedded and surface-mounted actuators has been extensively examined for actuators aligned with the beam axis; however, adequate torsion models are not available.

This paper further explores formulation of one-dimensional torsion models by investigating warping functions, shear lag, and experimental strain and deflection data. First, an analytical model is developed with warping considerations but without shear lag effects to illuminate the influence of warping terms on the response. Second, shear lag is introduced to attenuate bending, extension, and torsion responses. Configurations with actuators on only one surface (asymmetric) and with actuators on both surfaces (symmetric) are developed by using both Bernoulli–Euler and uniform strain displacement assumptions for the actuator. Finally, issues associated with constraining the global system response to a one-dimensional framework are explored and further illustrated by experimental strain and deflection surveys, which also serve to validate the analytical models.

Analytical Models

The principle of virtual work is invoked to construct all of the models presented within this paper. Cross-sectional warping and shear lag effects are incorporated into the models and evaluated relative to those that do not capture such behavior. For illustrative purposes, detailed results are derived for a thin isotropic beam with a surface-bonded piezoceramic actuator as shown in Fig. 1. All expressions are derived in the absence of external forces and temperature gradients.

This model assumes that the structure behaves as a Bernoulli–Euler beam in bending and extension as shown in Fig. 2. Torsion is introduced by utilizing a cross-sectional warping function, λ, as suggested by Gjelsvik,[8] which is dependent upon the cross-sectional geometry of the structure. Adhesive shear lag effects are not included in this model. The assumed displacement field for the structure is given as

$$u = u_o - zw_{,x} - \lambda\phi_{,x} \tag{1a}$$

$$v = -z\phi \tag{1b}$$

$$w = w_o + y\phi \tag{1c}$$

where the warping function $\lambda = \lambda(y, z)$. The nonzero beam strains are

$$\varepsilon_{xx} = u_{o,x} - zw_{,xx} - \lambda\phi_{,xx} \tag{2a}$$

$$\gamma_{zx} = (y - \lambda_{,z})\phi_{,x} \tag{2b}$$

$$\gamma_{xy} = -(z + \lambda_{,y})\phi_{,x} \tag{2c}$$

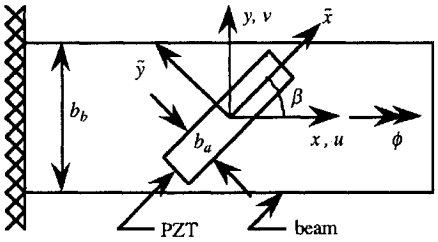

Fig. 1 Beam with surface-bonded piezoceramic.

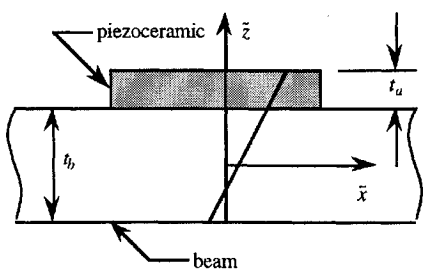

Fig. 2 Bernoulli–Euler axial deflections.

Assuming no external forces are applied, the principle of virtual work reduces to

$$\int_V \{\sigma_{xx}\delta\varepsilon_{xx} + \tau_{xy}\delta\gamma_{xy}\}\,dV = 0 \tag{3}$$

Further assuming that the actuators are of high-aspect ratio, the piezoceramic is approximated as inducing a strain only in its longitudinal axis. The induced strain is thereby transformed to beam axes as

$$\Lambda_{xx} = \Lambda\cos^2\beta \qquad \Lambda_{xy} = \Lambda\sin\beta\cos\beta \tag{4}$$

Utilizing the constitutive relationships

$$\sigma_{xx} = E(\varepsilon_{xx} - \Lambda\cos^2\beta) \tag{5a}$$

$$\tau_{zx} = G\gamma_{zx} \tag{5b}$$

$$\tau_{xy} = G(\gamma_{xy} - \Lambda\sin\beta\cos\beta) \tag{5c}$$

and separating the volume integral by subcomponents provides the expression

$$\int_{\text{beam}} \{E_b\varepsilon^b_{xx}\delta\varepsilon^b_{xx} + G_b\gamma^b_{zx}\delta\gamma^b_{zx} + G_b\gamma^b_{xy}\delta\gamma^b_{xy}\}\,dV + \int_{\text{actuator}} \{E_a(\varepsilon^a_{xx} - \Lambda\cos^2\beta)\delta\varepsilon^a_{xx} + G_a\gamma^a_{zx}\delta\gamma^a_{zx} + G_a(\gamma^a_{xy} - \Lambda\sin\beta\cos\beta)\delta\gamma^a_{xy}\}\,dV = 0 \tag{6}$$

For a rectangular beam with a piezoceramic bonded to one surface at orientation angle β, the warping function is approximated as

$$\lambda = kyz \tag{7}$$

The displacement warping formulation (7) exactly recovers the stress function presented by Timoshenko[9] for a thin rectangular bar. For an isotropic beam, $k = 1$. Substitution of the strain-displacement equations into the principle of virtual work and integrating provides the force boundary conditions and governing partial differential equations, which must be solved numerically. If the warping terms are ignored, except in correction of the shear strain term, and the substitution over variables given in Eq. (8) is introduced, the system response may be solved directly as given by Eq. (9):

$$\begin{aligned}
&\int_L \{E_bA_bu_{o,x}\delta u_{o,x} + E_bI^b_{yy}w_{,xx}\delta w_{,xx} + E_bI^b_{\lambda\lambda}\phi_{,xx}\delta\phi_{,xx} + G_bJ_b\phi_{,x}\delta\phi_{,x}\}\,dx \\
&+ \int_L \Big\{E_a\Big[A^*_a(u_{o,x} - \bar{z}_aw_{,xx} - x\bar{z}_a\tan\beta\phi_{,xx})\delta u_{o,x} \\
&+ I^*_a\Big(-\frac{\bar{z}_aA^*_a}{I^*_a}u_{o,x} + w_{,xx} + x\tan\beta\phi_{,xx}\Big)\delta w_{,xx} \\
&+ (-x\bar{z}_aA^*_a\tan\beta u_{o,x} + xI^*_a\tan\beta w_{,xx} + I^a_{\lambda\lambda}\phi_{,xx})\delta\phi_{,xx}\Big] \\
&+ G_aJ^*_a\phi_{,x}\delta\phi_{,x}\Big\}\,dx \\
&- \int_L \{E_aA^*_a\Lambda\cos^2\beta\delta u_{,x} - \bar{z}_aE_aA^*_a\Lambda\cos^2\beta\delta w_{,xx} \\
&- x\bar{z}_aE_aA^*_a\Lambda\sin\beta\cos\beta\delta\phi_{,xx}
\end{aligned}$$

where

$$\varepsilon_o = u_{,x} \qquad \kappa = w_{,xx} \qquad \theta = \phi_{,x} \tag{8}$$

$$\begin{bmatrix} EA & ES & 0 \\ ES & EI & 0 \\ 0 & 0 & GJ \end{bmatrix} \begin{Bmatrix} \varepsilon_o \\ \kappa \\ \theta \end{Bmatrix} = \begin{Bmatrix} P \\ M \\ T \end{Bmatrix} \tag{9}$$

where

$$EA = \iint_A E\,dy\,dz = E_b A_b + E_a A_a^* \tag{10a}$$

$$ES = -\iint_A Ez\,dy\,dz = -\bar{z}_a E_a A_a^* \tag{10b}$$

$$EI = -\iint_A Ez^2\,dy\,dz = E_b I_b + E_a I_a^* \tag{10c}$$

$$GJ = \iint_A G\left[(y-\lambda_{,z})^2 + (z+\lambda_{,y})^2\right] dy\,dz = G_b J_b + G_a J_a^* \tag{10d}$$

$$P = \iint_A \Lambda E\,dy\,dz = E_a A_a^* \Lambda \cos^2\beta \tag{10e}$$

$$M = -\iint_A \Lambda Ez\,dy\,dz = -\bar{z}_a E_a A_a^* \Lambda \cos^2\beta \tag{10f}$$

$$T = \iint_A \Lambda G[(y-\lambda_{,z}) - (z+\lambda_{,y})]\,dy\,dz$$

$$= -2\bar{z}_a G_a A_a^* \Lambda \sin\beta\cos\beta \tag{10g}$$

$$A_a^* = b_a t_a / \cos\beta \tag{11a}$$

$$I_a^* = \frac{1}{\cos\beta}\left(\frac{b_a t_a^3}{12} + \bar{z}_a^2 b_a t_a\right) \tag{11b}$$

$$I_{\lambda\lambda}^a = \left(x^2\tan^2\beta + \frac{b_a^2}{12\cos^2\beta}\right) I_{yy}^a \tag{11c}$$

$$J_a^* = 4I_a^* \tag{11d}$$

$$A_b = b_b t_b \tag{11e}$$

$$I_{\lambda\lambda}^b = \tfrac{1}{12} b_a t_a^3 \tag{11f}$$

$$I_{\lambda\lambda}^b = \tfrac{1}{144} A_b^3 \tag{11g}$$

$$J_b = \tfrac{1}{3} b_b t_b^3 \tag{11h}$$

The governing equations with warping terms are solved by using the finite-element method for 1, 10, and 50 elements. The solution exhibits good convergence for a low number of elements as shown in Fig. 3. The torsional response has essentially converged for a single element, yet the bending response requires 10 elements. The assumed displacements for the basic beam finite element are given as a function of the nondimensional elemental coordinate s as

$$u(s) = (1-s)u_1 + su_3 w(s)$$

$$= (2s^3 - 3s^2 + 1)w_1 + l(s^3 - 2s^2 + s)w_1' \tag{12a}$$

$$+ (-2s^3 + 3s^2)w_3 + l(s^3 - s^2)w_3' \tag{12b}$$

$$\phi(s) = (2s^2 - 3s + 1)\phi_1 + (-4s^2 + 4s)\phi_2 + (2s^2 - s)\phi_3 \tag{12c}$$

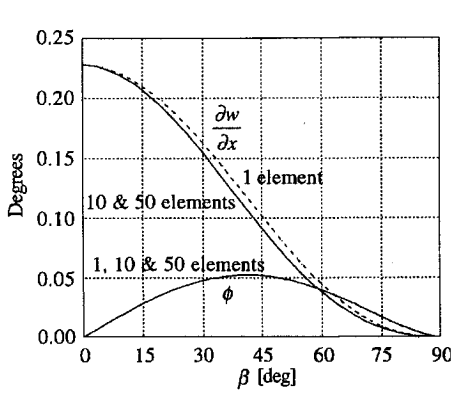

Fig. 3 Solution convergence.

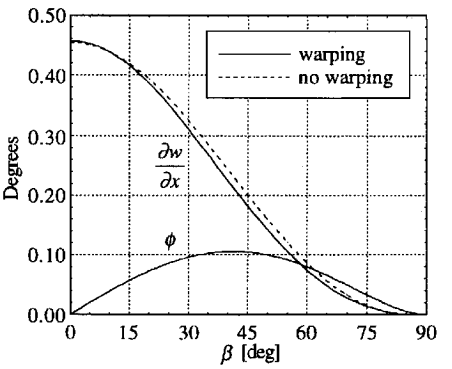

Fig. 4 Effects of warping terms.

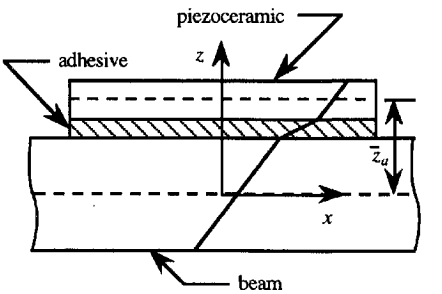

Fig. 5 Axial displacement variation with bond layer.

The effects of the warping terms that result in extension-twist and bending-twist elastic couplings are shown in Fig. 4 for a $2L^* \times 2.00 \times 0.0305$ in. ($2L^* \times 50.8 \times 0.77$ mm) aluminum beam with two asymmetrically bonded $1.85 \times 0.50 \times 0.0093$ in. ($47 \times 12.7 \times 0.236$ mm) G-1195 piezoceramics subjected to a $-175\ \mu\varepsilon$ actuation strain. L^* is the characteristic actuator half-length given by the projection of one-half of the actuator length onto the beam axis. For this case of a thin rectangular isotropic bar, the warping effects are negligible.

Shear Lag Model

In formulating a shear lag model, the configuration of an isotropic beam with a single surface-bonded piezoceramic, such as previously shown in Fig. 1, is considered. Because structural couplings due to warping terms are negligible for this type of structure, cross-sectional warping is considered only to correct the actuator shear strain. The effects of a finite thickness bond layer are considered by allowing the adhesive substrate to react to shear loads. Extensional displacements are shown in Fig. 5. The displacement field is assumed to be

$$u_b = u_b^o - zw_{b,x}^o - yz\phi_{b,x} \tag{13a}$$

$$v_b = -z\phi_b \tag{13b}$$

$$w_b = w_b^o + y\phi_b \tag{13c}$$

$$u_a = u_a^o - (z - \bar{z}_a)w_{b,x}^o - yz\phi_{a,x} \tag{14a}$$

$$v_a = -z\phi_a \tag{14b}$$

$$w_a = w_b^o + y\phi_a \tag{14c}$$

where $\bar{z}_a$ is the location of the actuator midplane with reference to the beam midplane. If we neglect the warping terms in the beam and actuator extensional strains, the nonzero strains become

$$\varepsilon_{xx}^b = u_{b,x}^o - zw_{b,xx}^o \tag{15a}$$

$$\gamma_{xy}^b = -2z\phi_{b,x} \tag{15b}$$

$$\varepsilon_{xx}^a = u_{a,x}^o - (z - \bar{z}_a)w_{b,xx}^o \tag{15c}$$

$$\gamma_{xy}^a = -2z\phi_{a,x} \tag{15d}$$

The adhesive shear strains are related to the differential extension and twist of the beam and actuator. The displacements through the adhesive thickness are linear interpolations between the actuator and beam displacements at the adhesive substrate interfaces. The shear due to bending and extension deformation is

$$\gamma_{zx}^{s} = \frac{1}{t_s}\left(u_a^o - u_b^o + \frac{t_a + t_b}{2} w_{b,x}^o\right) \tag{16}$$

The torsional shear is assumed to be due to a similar difference in transverse displacement except that both the actuator and beam undergo rigid body translations only as given by the displacement field. Hence, the torsional adhesive shear strain is given by

$$\gamma_{yz}^{s} = (1/t_s)\{[t_s + (t_b/2)]\phi_a - (t_b/2)\phi_a\} \tag{17}$$

Invoking the principle of virtual work with the induced strain assumption given previously by Eq. (4) provides the governing differential equations (18) through (22) and associated force boundary conditions (23) through (28) applied at $x = \pm(l/2)\cos\beta$. Note that the y-axis limits of integration are $y = x\tan\beta \pm (b_a/2)\cos\beta$ and begin to break down at high orientation angles:

$$E_a A_a^* u_{a,xx}^o - \frac{G_s A_s^*}{t_s^2}\left(u_a^o - u_b^o + \frac{t_a + t_b}{2} w_{b,x}^o\right) = 0 \tag{18}$$

$$E_b A_b u_{b,xx}^o + \frac{G_s A_s^*}{t_s^2}\left(u_a^o - u_b^o + \frac{t_a + t_b}{2} w_{b,x}^o\right) = 0 \tag{19}$$

$$\left(E_b I_b + E_a I_a^*\right) w_{b,xxxx}^o - \frac{G_s A_s^*}{t_s^2}\frac{t_a + t_b}{2}\left(u_{a,x}^o - u_{b,x}^o + \frac{t_a + t_b}{2} w_{,xx}\right) = 0 \tag{20}$$

$$G_a J_a^* \phi_{a,xx} - \frac{G_a A_s^*}{t_s^2}\left(t_s + \frac{t_b}{2}\right)\left[\left(t_s + \frac{t_b}{2}\right)\phi_a - \frac{t_b}{2}\phi_b\right] = 0 \tag{21}$$

$$G_b J_b \phi_{a,xx} + \frac{G_a A_s^*}{t_s^2}\frac{t_b}{2}\left[\left(t_s + \frac{t_b}{2}\right)\phi_a - \frac{t_b}{2}\phi_b\right] = 0 \tag{22}$$

$$E_a A_a^* u_{a,x}^o = E_a A_a^* \Lambda \cos^2\beta \tag{23}$$

$$E_b A_b u_{b,x}^o = 0 \tag{24}$$

$$\left(E_b I_b + E_a I_a^*\right) w_{,xx} = 0 \tag{25}$$

$$\left(E_b I_b + E_a I_a^*\right) w_{,xxx} - \frac{G_s A_s^*}{t_s^2}\frac{t_a + t_b}{2}\left(u_a^o - u_b^o + \frac{t_a + t_b}{2} w_{,x}\right) = 0 \tag{26}$$

$$G_a J_a^* \phi_{a,x} = -2\bar{z}_a G_a A_a^* \Lambda \sin\beta\cos\beta \tag{27}$$

$$G_b J_b \phi_{b,x} = 0 \tag{28}$$

where

$$A_a^* = \frac{b_a t_a}{\cos\beta} \qquad J_a^* = \frac{1}{\cos\beta}\left(\frac{1}{3} b_a t_a^3 + 4\bar{z}_a^2 b_a t_a\right)$$

$$A_b = b_b t_b \qquad I_b = \frac{1}{12} b_b t_b^3 \qquad J_b = \frac{1}{3} b_b t_b^3 \tag{29}$$

$$A_s^* = \frac{b_s t_s}{\cos\beta} \qquad \bar{z}_a = t_s + \frac{t_a + t_b}{2}$$

Note that the torsion equations are not coupled with the bending and extension equations.

Torsional Solution

By increasing the order of the torsion system of equations, given by Eqs. (21) and (22), the characteristic equation (30) is obtained:

$$D^2\left\{D^2 - \frac{G_s A_s}{t_s^2 \cos\beta}\left[\frac{\cos\beta}{G_a J_a}\left(t_s + \frac{t_b}{2}\right)^2 + \frac{1}{G_b J_b}\frac{t_b^2}{4}\right]\right\} = 0 \tag{30}$$

The solutions are, therefore, of the form

$$\phi_a = a_0 + a_1\bar{x} + a_2\cosh\Gamma_\phi\bar{x} + a_3\sinh\Gamma_\phi\bar{x} \tag{31}$$

$$\phi_b = b_0 + b_1\bar{x} + b_2\cosh\Gamma_\phi\bar{x} + b_3\sinh\Gamma_\phi\bar{x} \tag{32}$$

where the torsional shear lag parameter Γ_ϕ and the characteristic length L^* are defined as

$$\Gamma_\phi^2 = (L^*)^2 \frac{G_s A_s^*}{t_s^2}\left[\frac{1}{G_a J_a^*}\left(t_s + \frac{t_b}{2}\right)^2 + \frac{1}{G_b J_b}\frac{t_b^2}{4}\right] \tag{33}$$

$$L^* = (l/2)\cos\beta \tag{34}$$

Because the original equations are second order, only four of the eight coefficients are independent. Substitution of the solutions into either governing equation provides the dependency relations. By utilizing the force boundary conditions (27) and (28) and the cantilevered geometric boundary condition

$$\phi_b(\bar{x} = -1) = 0 \tag{35}$$

the final solutions are found to be

$$\phi_a = -\frac{TL^*}{GJ^*}\left[\frac{t_b}{2t_s + t_b}(\bar{x} + 1) + \frac{2t_s + t_b}{t_b}\frac{G_b J_b}{G_a J_a^*} \times \left(\frac{\sinh\Gamma_\phi\bar{x}}{\Gamma_\phi\cosh\Gamma_\phi} + \frac{\tanh\Gamma_\phi}{\Gamma_\phi}\right)\right] \tag{36}$$

$$\phi_b = -\frac{TL^*}{GJ^*}\left(\bar{x} + 1 - \frac{\sinh\Gamma_\phi\bar{x}}{\Gamma_\phi\cosh\Gamma_\phi} - \frac{\tanh\Gamma_\phi}{\Gamma_\phi}\right) \tag{37}$$

$$GJ^* = \frac{t_b}{2t_s + t_b} G_a J_a^* + \frac{2t_s + t_b}{t_b} G_b J_b \tag{38}$$

$$T = -2\bar{z}_a G_a A_a^* \Lambda \sin\beta\cos\beta \tag{39}$$

Unlike warping, the effects of the shear layer on a rectangular beam may be significant, as shown in Fig. 6 for a 2.00 × 0.0305 in. (50.8 × 0.77 mm) aluminum beam with a single 1.85 × 0.50 × 0.0093 in. (47 × 12.7 × 0.236 mm) G-1195 piezoceramics bonded to one surface. Note that the maximum twist occurs when the actuator orientation is near 45 deg.

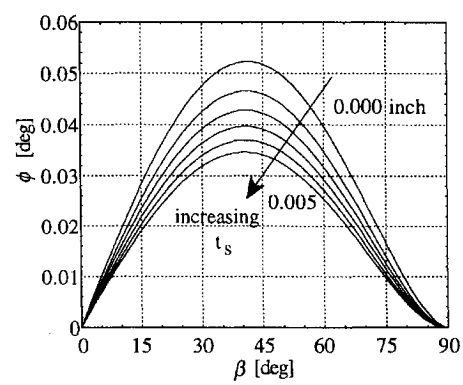

Fig. 6 Shear lag effects on twist response with bond thickness increasing from 0 to 0.005 in. (0.127 mm).

Extension-Bending Solution

Differentiating Eqs. (18–20) with respect to x and making the change of variables

$$\varepsilon_a^o = u_{a,x}^o \qquad \varepsilon_b^o = u_{b,x}^o \qquad \kappa = w_{,xx} \tag{40}$$

the system is represented in terms of the actuator midplane strain ε_a^o, beam midplane strain ε_b^o, and bending curvature κ. Solving the transformed system subject to boundary conditions (23–25) provides the solutions (41–43):

$$\varepsilon_a^o(\bar{x}) = \Lambda \cos^2\beta\left(\psi_a \frac{\cosh\Gamma_u\bar{x}}{\cosh\Gamma_u} + \psi_b + \psi_k\right) \tag{41}$$

$$\varepsilon_b^o(\bar{x}) = \Lambda\psi_b \cos^2\beta\left(1 - \frac{\cosh\Gamma_u\bar{x}}{\cosh\Gamma_u}\right) \tag{42}$$

$$\kappa(\bar{x}) = \Lambda\psi_\kappa \frac{2}{t_a + t_b}\cos^2\beta\left(\frac{\cosh\Gamma_u\bar{x}}{\cosh\Gamma_u} - 1\right) \tag{43}$$

where the stiffness ratios and axial shear lag parameter are defined as

$$\psi_a = \frac{1}{E_aA_a^*}\left[\frac{1}{E_aA_a^*} + \frac{1}{E_bA_b} + \frac{1}{4}\frac{(t_a+t_b)^2}{E_bI_b + E_aI_a^*}\right]^{-1} \tag{44a}$$

$$\psi_b = \frac{1}{E_bA_b}\left[\frac{1}{E_aA_a^*} + \frac{1}{E_bA_b} + \frac{1}{4}\frac{(t_a+t_b)^2}{E_bI_b + E_aI_a^*}\right]^{-1} \tag{44b}$$

$$\psi_\kappa = \frac{1}{4}\frac{(t_a+t_b)^2}{E_bI_b + E_aI_a^*}\left[\frac{1}{E_aA_a^*} + \frac{1}{E_bA_b} + \frac{1}{4}\frac{(t_a+t_b)^2}{E_bI_b + E_aI_a^*}\right]^{-1} \tag{44c}$$

$$\Gamma_u^2 = (L^*)^2\frac{G_sA_s^*}{t_s^2}\left[\frac{1}{E_aA_a^*} + \frac{1}{E_bA_b} + \frac{1}{4}\frac{(t_a+t_b)^2}{E_bI_b + E_aI_a^*}\right] \tag{44d}$$

$$L^* = (l/2)\cos\beta \tag{44e}$$

Integrating the beam curvature with respect to $\bar{x}$ and assuming the beam is cantilevered at $\bar{x} = -1$,

$$w_{,x}(\bar{x}) = \Lambda\psi_\kappa L^*\frac{2}{t_a + t_b}\cos^2\beta\left(\frac{\sinh\Gamma_u\bar{x}}{\Gamma_u\cosh\Gamma_u} + \frac{\tanh\Gamma_u}{\Gamma_u} - 1 - \bar{x}\right) \tag{45}$$

Unlike the torsional response, the effects of shear lag are much less on the bending slope as shown in Fig. 7 for a 2.00 × 0.0305 in. (50.8 × 0.77 mm) aluminum beam with a single 1.85 × 0.50 × 0.0093 in. (47 × 12.7 × 0.236 mm) G-1195 piezoceramics bonded to one surface. Adhesive thicknesses are 0.001 and 0.005 in. (0.025 and 0.127 mm), and the actuation strain is 175 $\mu\varepsilon$. The impact of shear lag is less severe on the bending slope than on the twist angle.

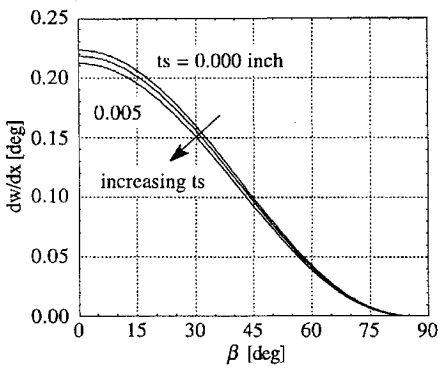

Fig. 7 Shear lag effects on extension–bending with bond thickness increasing from 0 to 0.005 in. (0.127 mm).

If the strain through the actuator is assumed to be uniform instead of linear, Eqs. (18–20) become

$$E_aA_a^*u_{a,xx}^o - \frac{G_sA_s^*}{t_s^2}\left(u_a^o - u_b^o + \frac{t_b}{2}w_{b,x}^o\right) = 0 \tag{46}$$

$$E_bA_bu_{b,xx}^o + \frac{G_sA_s^*}{t_s^2}\left(u_a^o - u_b^o + \frac{t_b}{2}w_{b,x}^o\right) = 0 \tag{47}$$

$$E_bI_bw_{b,xxxx}^o - \frac{G_sA_s^*}{t_s^2}\frac{t_b}{2}\left(u_{a,x}^o - u_{b,x}^o + \frac{t_b}{2}w_{b,xx}^o\right) = 0 \tag{48}$$

and the corresponding solutions are

$$\varepsilon_a^o(\bar{x}) = \Lambda \cos^2\beta\left(\psi_a \frac{\cosh\Gamma_u\bar{x}}{\cosh\Gamma_u} + \psi_b + \psi_k\right) \tag{49}$$

$$\varepsilon_b^o(\bar{x}) = \Lambda\psi_b \cos^2\beta\left(1 - \frac{\cosh\Gamma_u\bar{x}}{\cosh\Gamma_u}\right) \tag{50}$$

$$\kappa(\bar{x}) = -\Lambda\psi_\kappa \cos^2\beta\frac{2}{t_b}\left(1 - \frac{\cosh\Gamma_u\bar{x}}{\cosh\Gamma_u}\right) \tag{51}$$

where the stiffness ratios and shear lag parameter are defined by

$$\psi_a = \frac{1}{E_aA_a^*}\left(\frac{1}{E_aA_a^*} + \frac{1}{E_bA_b} + \frac{t_b^2}{4}\frac{1}{E_bI_b}\right)^{-1} \tag{52a}$$

$$\psi_b = \frac{1}{E_bA_b}\left(\frac{1}{E_aA_a^*} + \frac{1}{E_bA_b} + \frac{t_b^2}{4}\frac{1}{E_bI_b}\right)^{-1} \tag{52b}$$

$$\psi_\kappa = \frac{t_b^2}{4}\frac{1}{E_bI_b}\left(\frac{1}{E_aA_a^*} + \frac{1}{E_bA_b} + \frac{t_b^2}{4}\frac{1}{E_bI_b}\right)^{-1} \tag{52c}$$

$$\Gamma_u^2 = (L^*)^2\frac{G_sA_s^*}{t_s^2}\left(\frac{1}{E_aA_a^*} + \frac{1}{E_bA_b} + \frac{t_b^2}{4}\frac{1}{E_bI_b}\right) \tag{53}$$

The torsional response is unaffected by this change in assumed displacement. The effects of a uniform vs linear actuator strain are shown in Fig. 8 for two orientation angles for a 2.0 × 0.0305 in. (50.8 × 0.77 mm) aluminum beam with a surface bonded 1.85 × 0.50 × t_a in. (47 × 12.7 × t_a) G-1195. For $\beta = 0$ deg, the difference between the two curvatures is >5% for thickness ratios below 18 and >10% for ratios below 7. The Bernoulli–Euler strain distribution predicts no bending as the beam thickness vanishes. This result is consistent with the behavior of real beams and the results of Crawley and Anderson.[6] Note that the curvature for the beam is greater for $\beta = 0$ deg than for $\beta = 45$ deg. The reduction in curvature is attributed to attenuated actuation strain in the beam axis direction.

Symmetric Configuration

If an actuator is added to the bottom surface of the previous configuration and oriented at $-\beta$, then the structural response will be a coupled extension–twist motion provided that both actuators extend

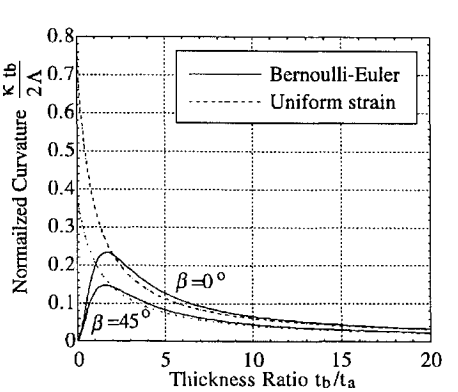

Fig. 8 Effects of actuator bending.

or both contract. By using the previous solution methodology, the torsional response is similar to that of Eqs. (36) and (37):

$$\phi_a = -\frac{TL^*}{GJ^*}\left[\frac{t_b}{2t_s + t_b}(\bar{x} + 1) + \frac{2t_s + t_b}{t_b}\frac{G_b J_b}{2G_a J_a^*}\left(\frac{\sinh \Gamma_\phi \bar{x}}{\Gamma_\phi \cosh \Gamma_\phi} + \frac{\tanh \Gamma_\phi}{\Gamma_\phi}\right)\right] \tag{54}$$

$$\phi_b = -\frac{TL^*}{GJ^*}\left[\bar{x} + 1 - \frac{\sinh \Gamma_\phi \bar{x}}{\Gamma_\phi \cosh \Gamma_\phi} - \frac{\tanh \Gamma_\phi}{\Gamma_\phi}\right] \tag{55}$$

The axial response is derived as

$$u_a^o(\bar{x}) = \frac{PL^*}{EA^*}(\bar{x} + 1) + \frac{PL^*}{EA^*}\frac{E_b A_b}{2E_a A_a^*}\left(\frac{\sinh \Gamma_u \bar{x}}{\Gamma_u \cosh \Gamma_u} - \frac{\tanh \Gamma_u}{\Gamma_u}\right) \tag{56}$$

$$u_b^o(\bar{x}) = \frac{PL^*}{EA^*}\left(\bar{x} + 1 - \frac{\sinh \Gamma_u \bar{x}}{\Gamma_u \cosh \Gamma_u} - \frac{\tanh \Gamma_u}{\Gamma_u}\right) \tag{57}$$

$$\varepsilon_a^o(\bar{x}) = \frac{P}{EA^*}\left(1 + \frac{E_b A_b \cos \beta}{2E_a A_a}\frac{\cosh \Gamma_u \bar{x}}{\cosh \Gamma_u}\right) \tag{58}$$

$$\varepsilon_b^o(\bar{x}) = \frac{P}{EA^*}\left(1 - \frac{\cosh \Gamma_u \bar{x}}{\cosh \Gamma_u}\right) \tag{59}$$

where

$$GJ^* = \frac{2t_b}{2t_s + t_b}G_a J_a^* + \frac{2t_s + t_b}{t_b}G_b J_b \tag{60}$$

$$EA^* = 2E_a A_a^* + E_b A_b \tag{61}$$

$$T = -4\bar{z}_a G_a A_a^* \Lambda \sin \beta \cos \beta \tag{62}$$

$$P = 2E_a A_a^* \Lambda \cos^2 \beta \tag{63}$$

$$\Gamma_u^2 = (L^*)^2 \frac{G_s A_s^*}{t_s^2}\left[\frac{1}{2E_a A_a^*} + \frac{1}{E_b A_b}\right] \tag{64}$$

$$\Gamma_\phi^2 = (L^*)^2 \frac{G_s A_s^*}{t_s^2}\left[\frac{1}{2G_a J_a^*}\left(t_s + \frac{t_b}{2}\right)^2 + \frac{1}{G_b J_b}\frac{t_b^2}{4}\right] \tag{65}$$

The twist rate for a symmetric specimen is not quite twice that of an asymmetric one as shown in Fig. 9 for a 2.00 × 0.0305 in. (50.8 × 0.77 mm) aluminum beam with three and six 1.85 × 0.25 × 0.0093 in. (47 × 12.7 × 0.236 mm) G-1195 piezoceramics for the asymmetric and symmetric cases, respectively. The induced torque is exactly doubled; however, the torsional stiffness exhibits an increase because of the additional piezoceramic stiffness. In the limit of a thick beam with thin piezoceramics, the symmetric twist response approaches twice the asymmetric twist.

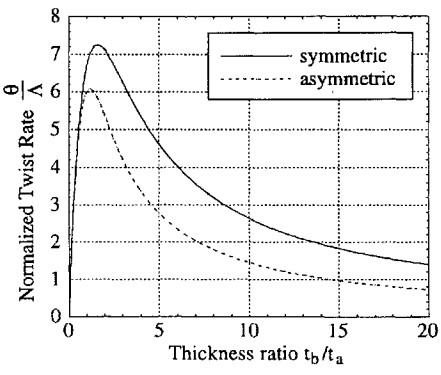

Fig. 9 Twist rate comparison.

One-Dimensional Platform Constraints

The global response of a high aspect ratio structure, such as a rotor blade, is adequately characterized by beam behavior. In addition to mathematical simplicity and physical understanding, modeling of induced torsion of beams is preferably constrained to a one-dimensional response. Because the actuation mechanism is inherently a two-dimensional phenomenon, means by which to incorporate these two-dimensional piezoceramic effects into a global one-dimensional response model are not established, especially for arbitrary actuator geometries. In the limiting case of high aspect ratio actuators with simple geometry, the actuation mechanics simplify appreciably. The limitations of such reductions are difficult to quantify analytically, thereby requiring experimental methods to identify limits of applicability.

There exist several approaches by which to capture piezoceramic actuation in a beam model, each of which has different strengths and weaknesses. The models presented in this paper assume that the piezoceramic induces strain only in its longitudinal axis, which is oriented by angle β with respect to the beam axis. Effectively, this is an assumption on material properties and conflicts with the basic physics of torsion actuation of a beam. Intuitively, torsion should arise as a result of geometric constraints, because the considered piezoceramics exhibit isotropic in-plane characteristics. However, in the limit of high aspect ratio actuators, the utilized modification of material properties is a reasonable compromise for detailed geometric modeling.

The induced force and torque in the presented models are metrics by which to evaluate their effectiveness to actuator orientation. By assuming line element behavior of the piezoceramic, as done in this paper, the resulting force and torque expressions for the asymmetric configuration are

$$P = E_a A_a^* \Lambda \cos^2 \beta \tag{66}$$

$$T = -2\bar{z}_a G_a A_a^* \Lambda \sin \beta \cos \beta \tag{67}$$

If, instead, the piezoceramic is permitted full two-dimensional isotropic material properties, the stress–strain relations are given by

$$\begin{Bmatrix} \sigma_{\bar{x}\bar{x}}^a \\ \sigma_{\bar{y}\bar{y}}^a \\ \tau_{\bar{x}\bar{y}}^a \end{Bmatrix} = \frac{E_a}{1 - \nu_a^2}\begin{bmatrix} 1 & \nu_a & 0 \\ \nu_a & 1 & 0 \\ 0 & 0 & \dfrac{1 - \nu_a}{2} \end{bmatrix}\begin{Bmatrix} \varepsilon_{\bar{x}\bar{x}}^a - \Lambda \\ \varepsilon_{\bar{y}\bar{y}}^a - \Lambda \\ \gamma_{\bar{x}\bar{y}}^a \end{Bmatrix} \tag{68}$$

and the internal virtual work becomes

$$\delta U_a = \int_V \frac{E_a}{1 - \nu_a^2}\{[\varepsilon_{\bar{x}\bar{x}}^a + \nu_a \varepsilon_{\bar{y}\bar{y}}^a - (1 + \nu_a)\Lambda]\delta\varepsilon_{\bar{x}\bar{x}}^a + [\nu_a \varepsilon_{\bar{x}\bar{x}}^a + \varepsilon_{\bar{y}\bar{y}}^a - (1 + \nu_a)\Lambda]\delta\varepsilon_{\bar{y}\bar{y}}^a + [\nu_a \varepsilon_{\bar{x}\bar{x}}^a + \varepsilon_{\bar{y}\bar{y}}^a - (1 + \nu_a)\Lambda]\delta\varepsilon_{\bar{y}\bar{y}}^a\}\mathrm{d}V \tag{69}$$

Because the strain transverse to the beam axis is identically 0 as a result of beam behavior, the strain transformation becomes

$$\begin{Bmatrix} \varepsilon_{\bar{x}\bar{x}}^a \\ \varepsilon_{\bar{y}\bar{y}}^a \\ \gamma_{\bar{x}\bar{y}}^a \end{Bmatrix} = \begin{bmatrix} \cos^2 \beta & 2 \sin \beta \cos \beta \\ \sin^2 \beta & -2 \sin \beta \cos \beta \\ -\sin \beta \cos \beta & \cos^2 \beta - \sin^2 \beta \end{bmatrix}\begin{Bmatrix} \varepsilon_{xx}^a \\ \gamma_{xy}^a \end{Bmatrix} \tag{70}$$

Substituting (70) into the energy expression (69) and regrouping terms produces extension–twist coupling, which is proportional to $(\cos^2 \beta - \sin^2 \beta)$. Note that this coupling vanishes exactly when $\beta = 45$ deg. The resulting force and torque are obtained as

$$P = \Lambda \frac{E_a A_a^*}{1 - \nu_a} \tag{71}$$

$$T = 0 \tag{72}$$

Even though structural couplings between torsional and bending and extension responses due to the presence of a discrete actuator should be a maximum when $\beta = 45$ deg, no torsion arises. When we examine axial force equations (66) and (71), the underlying piezoceramic assumption effects become clear in the limiting configurations

of $\beta = 0$ and 90 deg. When $\beta = 0$ deg, the two forces are identical with the exception of the Poisson effect in (71), which is due to plate theory. Hence, both assumptions result in nearly the same bending response. When $\beta = 90$ deg, the assumption that modifies material properties produces exactly no response, whereas the one that utilizes isotropic properties generates the force that both assumptions would produce if the actuator dimensions were reversed and β was set to 0.

If transverse actuator stiffness is neglected, so that the actuator has orthotropic characteristics, the axial force and torque are

$$P = E_a A_a^* \Lambda \cos^2 \beta \tag{73}$$

$$T = 4\bar{z}_a E_a A_a^* \Lambda \cos \beta \sin \beta \tag{74}$$

Note that the axial force (73) is identical to (66), yet the induced torque is much higher and intuitively incorrect, which indicates that transverse actuator stiffness is relevant to obtaining sensible predictions.

The importance of including transverse actuator mechanics is clear in terms of the implications on the bending response, yet less so in terms of torsion. Transverse stiffness is essential in obtaining a correct induced torque, and two-dimensional piezoceramic properties are needed to correct the bending response at high orientation angles, $\beta > 45$ deg. Means by which such mechanics can be adequately incorporated into a one-dimensional framework are not developed. Hence, the bending predictions of the models within this paper are expected to break down at $\beta > 45$ deg. The impact of the underlying assumptions on the torsion response is not obvious and requires experimental studies for further insight.

Experimental Results

Strain and deflection data were collected for a variety of specimen parameters to understand more fully the micromechanics of the torsion problem as well as to provide correlation for the theoretical models. All of the specimens consisted of thin aluminum beams with surface-bonded piezoceramics. All deflection data were obtained by reflecting a laser beam off the tip of the specimen onto a surface approximately 20 ft (6 m) away. The vertical and horizontal displacements of the laser beam on this surface were measured and related to the angular rotations. Both G-1195 and PZT-5H piezoceramics were used in the experiments. Note that two separate lots of G-1195 piezoceramics exhibited different characteristics. The free strain of each type was individually characterized and approximated by a polynomial curve fit.

Tip twist angle and bending slope results were obtained for thin aluminum beam configurations with piezoceramics bonded to only one surface (asymmetric case) at angle β with respect to the beam axis. To obtain measurable results, multiple piezoceramics were required. Local interference effects were minimized by maintaining a 4-in. (101 mm) spacing between piezoceramics, and a principle of superposition was assumed. The asymmetric specimens with a piezoceramic aspect ratio of 8 consisted of three $2.0 \times 0.25 \times 0.0075$ in. ($50.8 \times 6.35 \times 0.19$ mm) G-1195(a) piezoceramics bonded to the same surface of 2.0×0.0312 in. (50.8×0.77 mm) aluminum beams. The bond layer thickness was measured to be 0.0015 in. (0.038 mm).

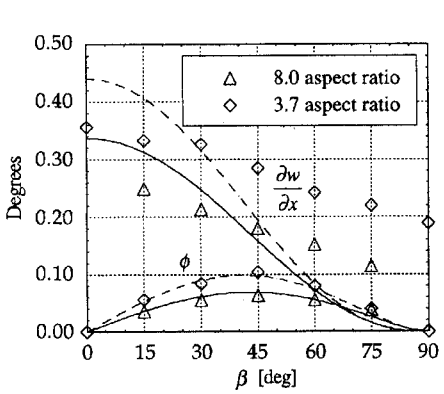

Fig. 10 Asymmetric torsion results comparison.

The asymmetric specimens with 3.7 aspect ratio piezoceramics consisted of two $1.85 \times 0.50 \times 0.0093$ in. ($47 \times 12.7 \times 0.236$ mm) G-1195(b) piezoceramics bonded to the same surface of 1.97×0.0305 in. (50×0.77 mm) aluminum beams. The measured adhesive thickness was 0.004 in. (0.10 mm).

The theoretical shear lag model predictions show good correlation with experimental results for the asymmetric case shown in Fig. 10 in torsional deflections. Bending slope predictions, however, rapidly deteriorate as the orientation angle increases but are acceptable up to $\beta = 45$ deg for both sets of specimens. The model considered the actuators as one-dimensional elements. Hence, the bending slope and twist angle are both expected to approach 0 at $\beta = 90$ deg. Because the true bending slope is finite at that limit and the twist angle is 0, the twist predictions are expected to be much better over the range of orientation angles.

To more fully understand the micromechanics of the beam response, strain gauge measurements were taken from several asymmetric test specimens with G-1195 and PZT-5H piezoceramics. Both the piezoceramic and beam surface opposite the piezoceramic side were instrumented to obtain detailed strain distributions.

As shown in Fig. 11a the lower-beam surface axial strain increases toward the edge of the actuator in the lengthwise direction. However, Fig. 11b shows that the strain exhibits relatively little decrease in the direction transverse to the actuator. The transverse strain, on the

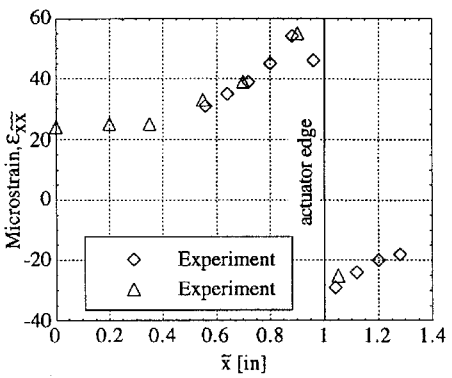

Fig. 11a Experimental variation of $\varepsilon_{\tilde{x}\tilde{x}}$.

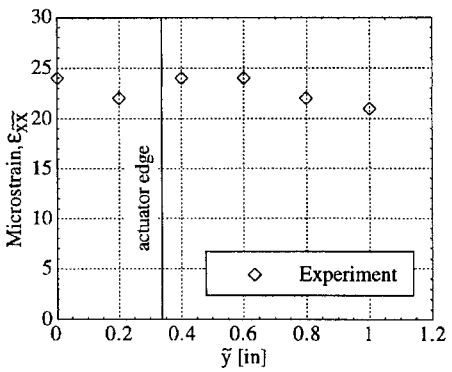

Fig. 11b Experimental variation of $\varepsilon_{\tilde{x}\tilde{x}}$.

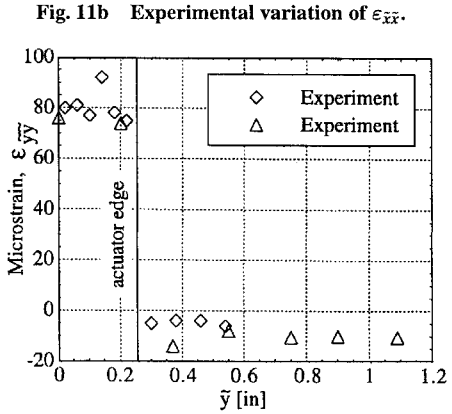

Fig. 11c Experimental variation of $\varepsilon_{\tilde{y}\tilde{y}}$.

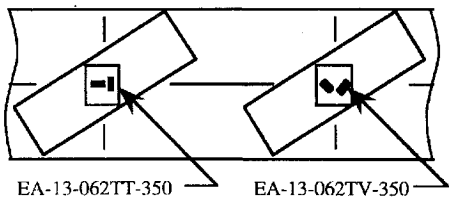

Fig. 12 Shear type gauge locations.

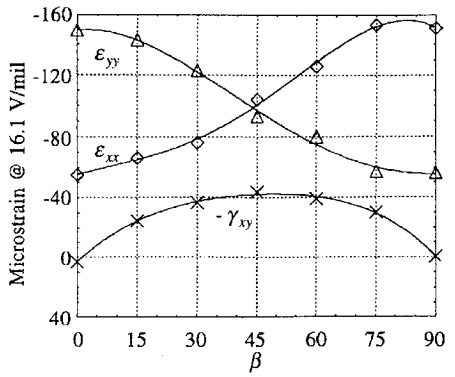

Fig. 13 Experimental piezoceramic surface strain.

other hand, is approximately constant across the actuator width as shown in Fig. 11c. All strain distributions were taken from 2.0 × 0.0312 in. (50.8 × 0.79 mm) aluminum beams with a single 2.0 × 0.50 × 0.0093 in. (50.8 × 12.7 × 0.236 mm) PZT-5H piezoceramic with $\beta = 45$ deg.

Several shear-type strain gauges were located at the center of the piezoceramics shown in Fig. 12 on the previous asymmetric specimens with 3.7 piezoceramic aspect ratios. Because the variation in piezoceramic thickness within a given set of specimens is ±0.1 mil and the deflection results exhibit a definable smooth trend, the four strain readings from a single specimen are deemed compatible for determining the total strain state for each specimen as if a rosette-type gauge were used. All measured strains were at 0, 45, 90, and 135 deg relative to the beam axis.

Experimental strain results are shown in Fig. 13 for an actuated strain of $-175\ \mu\varepsilon$. Fourth-order polynomial curve fits are overlaid on the test data to illustrate the trends more clearly. As shown, the shear strain is a maximum when $\beta = 45$ deg and is 0 at the two limits. The beam extension and transverse strains are mirrored about $\beta = 45$ deg. At the two extremes, the actuated and measured lateral strains are approximately equal, thereby indicating a small energy contribution. However, at 45 deg the transverse and longitudinal strains are approximately equal, thereby indicating a highly two-dimensional strain state and a breakdown of the one-dimensional piezoceramic modeling assumption.

Note that the conference paper provides detailed experimental specimen parameters and test results used in this paper, including the geometric parameters of the beam configurations, deflection and strain results, and the free strain characteristics of the piezoceramics used.[10] Also note that two separate batches of G-1195 piezoceramics from the same manufacturer exhibit significantly different induced strain characteristics.

Summary and Conclusions

This paper developed several variations of a model to predict the torsion, extension, and bending response of a beam subject to piezoceramic actuation and presented strain and deflection data to illustrate the mechanics of the problem and to provide model substantiation. In addition, issues associated with reducing two-dimensional piezoceramic characteristics to a one-dimensional model were explored. A finite element solution for the model with warping terms is shown to converge for a low number of elements. In the absence of warping terms and shear lag, the model reduces to a system of three equations that may be solved directly.

Torsion is introduced into the models by application of a cross-sectional warping function that is dependent only upon cross-sectional geometry. For isotropic rectangular beams, the effects of the warping terms in the axial strain expressions were shown to be negligible; however, the warping is important in terms of quantifying the shear strain. Adhesive shear lag effects also are developed and show a measurable impact on the results.

Adequately capturing the two-dimensional strain induction characteristics of the piezoceramics is critical in obtaining good predictions over a wide range of orientation angles. Modification of the piezoceramic material properties by neglecting transverse induced strain is inconsistent with the basic physics of the system but is a good approximation if high aspect ratios are maintained. Inclusion of the transverse induced strain results in a model that does not twist when $\beta = 45$ deg. Experimentally, the maximum twist occurs at this orientation angle. Completely neglecting transverse actuator stiffness results in adequate axial induced forces but greatly overestimates the induced torque. Therefore, allowing full in-plane isotropic piezoceramic characteristics may represent more accurately the true physics, but such assumptions are incompatible with the utilized beam theory.

Experimental deflection results exhibit fair correlation with model predictions for piezoceramic aspect ratios as low as 3.7. The theoretical bending predictions significantly deviate from experimental data above $\beta = 45$ deg, especially for the specimen with the lower aspect ratio piezoceramics. This divergence is inevitable, because theoretical predictions approach 0 for $\beta = 90$ deg, as opposed to the finite response obtained experimentally. More sophisticated means of reducing two-dimensional system behavior to a one-dimensional global platform, such as solving the full two-dimensional problem, would improve these results. Twist angle predictions, on the other hand, are accurate for the full range of permissible orientation angles. This is attributed to both theory and experiment being in exact agreement in the two limiting actuator orientations, unlike the bending response.

Detailed strain distributions indicate that transverse actuator and beam strain energy contributions are not negligible for all actuator orientations. However, experimental results indicate that two-dimensional modeling details are necessary only to correct the predictions for high actuator orientations. When $\beta < 45$ deg, the models presented here are considered sufficient to predict the bending and twist response of rectangular isotropic beams subject to induced strain actuation.

Acknowledgments

This work is supported by the U.S. Army Research Office under Grant DAAL 03-92-G-0121 with Gary Anderson as Technical Monitor. Experimental data were collected by the authors with assistance from Burtis Spencer.

References

[1]Nguyen, K., and Chopra, I., "Application of Higher Harmonic Control to Rotors Operating at High Speed and Thrust," *Journal of the American Helicopter Society*, Vol. 35, No. 3, 1990, pp. 78, 79.

[2]Chopra, I., and McCloud, J. C., III., "A Numerical Simulation Study of Open Loop, Closed Loop and Adaptive Multicyclic Control Systems," *Journal of the American Helicopter Society*, Vol. 28, No. 1, 1983, pp. 63–77.

[3]Ham, N. D., "Helicopter Individual-Blade-Control Research at MIT 1977–1985," *Vertica*, Vol. 11, No. 1/2, 1987, pp. 109–122.

[4]Crawley, E., and de Luis, J., "Use of Piezo-Ceramics as Distributed Actuators in Large Space Structures," *Proceedings of the AIAA 26th Structures, Structural Dynamics, and Materials Conference* (Orlando, FL), AIAA, New York, 1985, pp. 126–132.

[5]Crawley, E., and de Luis, J., "Use of Piezoelectric Actuators as Elements of Intelligent Structures," *AIAA Journal*, Vol. 25, No. 10, 1987, pp. 1373–1385.

[6]Crawley, E., and Anderson, E., "Detailed Models of Piezoceramic Actuations of Beams," *Journal of Intelligent Material Systems*, Vol. 1, No. 1, 1990, pp. 4–25.

[7]Park, C., Walz, C., and Chopra, I., "Bending and Torsion Models of Beams with Induced Strain Actuators," *Smart Materials and Structures*, Vol. 5, No. 1, 1996, pp. 98–113.

[8]Gjelsvik, A., *Theory of Thin Walled Bars*, Wiley-Interscience, New York, 1981, Chaps. 1, 2.

[9]Timoshenko, S., *Theory of Elasticity*, McGraw–Hill, New York, 1934.

[10]Park, C., and Chopra, I., "Modeling Piezoceramic Actuation of Beams in Torsion," *Proceedings of the AIAA 35th Structures, Structural Dynamics, and Materials Conference and Adaptive Structures Forum* (Hilton Head, SC), AIAA, Washington, DC, 1994, pp. 438–450.